

injection of UAS-Nkd constructs; and K. Cadigan and D. Bilder for stained material. W.Z. and J.M. were supported by postdoctoral training grants from the NIH and by the Howard Hughes Medical Institute (HHMI). K.A.W. was supported by an HHMI postdoctoral fellowship for physicians and a NIH K-08 Award. P.K. and M.P.S. are Investigators of the HHMI.

Correspondence and requests for materials should be addressed to M.P.S. (e-mail: scott@cmgm.stanford.edu). The *Drosophila nkd* cDNA has been deposited with GenBank (accession no. AF213376).

## Transcriptional silencing and longevity protein Sir2 is an NAD-dependent histone deacetylase

Shin-ichiro Imai, Christopher M. Armstrong, Matt Kaerberlein & Leonard Guarente

Department of Biology, Massachusetts Institute of Technology, Cambridge, Massachusetts 02139, USA

Yeast Sir2 is a heterochromatin component that silences transcription at silent mating loci<sup>1</sup>, telomeres<sup>2</sup> and the ribosomal DNA<sup>3,4</sup>, and that also suppresses recombination in the rDNA<sup>5</sup> and extends replicative life span<sup>6</sup>. Mutational studies indicate that lysine 16 in the amino-terminal tail of histone H4 and lysines 9, 14 and 18 in H3 are critically important in silencing, whereas lysines 5, 8 and 12 of H4 have more redundant functions<sup>7–9</sup>. Lysines 9 and 14 of histone H3 and lysines 5, 8 and 16 of H4 are acetylated in active chromatin and hypoacetylated in silenced chromatin, and overexpression of Sir2 promotes global deacetylation of histones<sup>9,10</sup>, indicating that Sir2 may be a histone deacetylase. Deacetylation of lysine 16 of H4 is necessary for binding the silencing protein, Sir3 (ref. 8). Here we show that yeast and mouse Sir2 proteins are nicotinamide adenine dinucleotide (NAD)-dependent histone deacetylases, which deacetylate lysines 9 and 14 of H3 and specifically lysine 16 of H4. Our analysis of two *SIR2* mutations supports the idea that this deacetylase activity accounts for silencing, recombination suppression and extension of life span *in vivo*. These findings provide a molecular framework of NAD-dependent histone deacetylation that connects metabolism, genomic silencing and ageing in yeast and, perhaps, in higher eukaryotes.

Sir2 is a limiting component that promotes longevity in yeast mother cells. Cells lacking Sir2 have a reduced replicative life span and cells with an extra copy of *SIR2* display a much longer life span than wild type<sup>6</sup>. This extension probably results from a hypersilencing in the rDNA which reduces recombination and the production of extrachromosomal rDNA circles, a known cause of senescence in ageing mother cells<sup>11</sup>. *SIR2* homologues have been identified in many organisms ranging from bacteria to humans<sup>12</sup>. The *Salmonella* homologue, *cobB*, has been implicated in a pyrimidine transfer reaction<sup>13</sup> and both CobB and eukaryotic Sir2 proteins possess ADP-ribosyltransferase activity<sup>14,15</sup>.

Because Sir2 proteins use NAD as a substrate in a ADP-ribosylation reaction, we examined whether NAD could be a co-factor necessary for deacetylase activity. We used purified recombinant Sir2 in a reaction with NAD and a peptide of the histone H3 N-terminal tail (residues 1–20) di-acetylated at lysines 9 and 14. We reacted 5 µg of recombinant yeast Sir2 (79 pmoles) (Fig. 1a), 10 µg of the H3 peptide (4.2 nmoles) and increasing concentrations of NAD and analysed the products by high-pressure liquid chromatography (HPLC). The peptide that reacted in the absence of NAD gave

rise to two peaks (3 and 5), which were analysed by mass spectroscopy (Fig. 1b; and Supplementary Information) and correspond to a monomeric (relative molecular mass ( $M_r$ ) 2370) and a dimeric ( $M_r$  4740) peptide, the latter probably due to oxidation of the peptide at the carboxyl cysteine residue. The same species were observed in reactions with a control bacterial preparation ('pET' in Fig. 1a) in the presence of NAD.

The addition of NAD to the reaction containing Sir2 gave rise to three additional peaks (1, 2 and 4) and an alteration in peak 3, which were also analysed by mass spectroscopy (Fig. 1c–f; and Supplementary Information). These peaks did not correspond to ADP-ribosylated species, but, rather, to deacetylated species of peptide (Fig. 1g). Peak 4 corresponded to the singly deacetylated dimer ( $M_r$  4698); peak 3 also contained the doubly deacetylated dimer ( $M_r$  4656); peak 2 corresponded to the triply deacetylated dimer ( $M_r$  4614), and peak 1 to the singly deacetylated monomer ( $M_r$  2328). We estimate that at least 27% of the input peptide was deacetylated

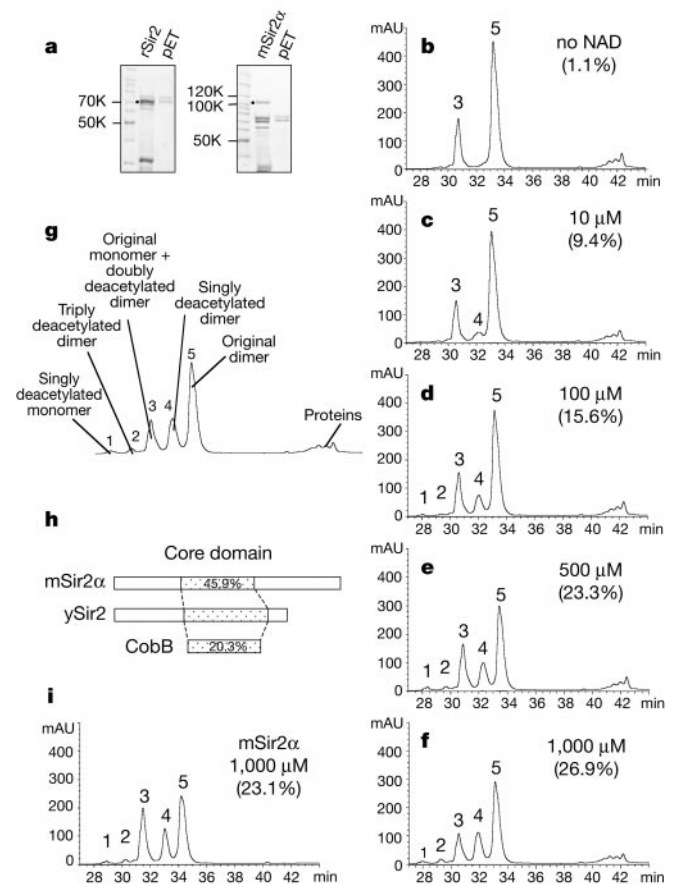


**Figure 1** *In vitro* deacetylation assays of the H3 peptide (residues 1–20) di-acetylated at lysines 9 and 14 by recombinant yeast Sir2. **a**, Coomassie blue-stained gel after SDS-PAGE of purified recombinant yeast (rSir2) and mouse Sir2 (mSir2 $\alpha$ ) proteins. Full-length proteins are indicated by dots. Vector controls (pET) were prepared analogously to recombinant proteins. **b–f**, HPLC chromatograms showing absorbance at 220 nm of products of deacetylation assays with yeast Sir2 and the indicated concentrations of NAD. The efficiencies of the reactions are calculated as a fraction of the areas under peaks 1, 2 and 4, compared with the area under all of the peaks. **g**, Contents of peaks 1–5. From the relative abundances of peaks, the dimer peptide is probably a better substrate than the monomer for Sir2. **h**, Comparison of mSir2 $\alpha$ , yeast Sir2 (ySir2) and CobB. Core domains are shown as shaded boxes with the percentages of amino-acid identity to the ySir2 core domain. **i**, The HPLC chromatogram of the product of deacetylation assay with 10 µg of recombinant mSir2 $\alpha$  protein at 1 mM NAD. The calculated efficiency of the reaction is indicated.

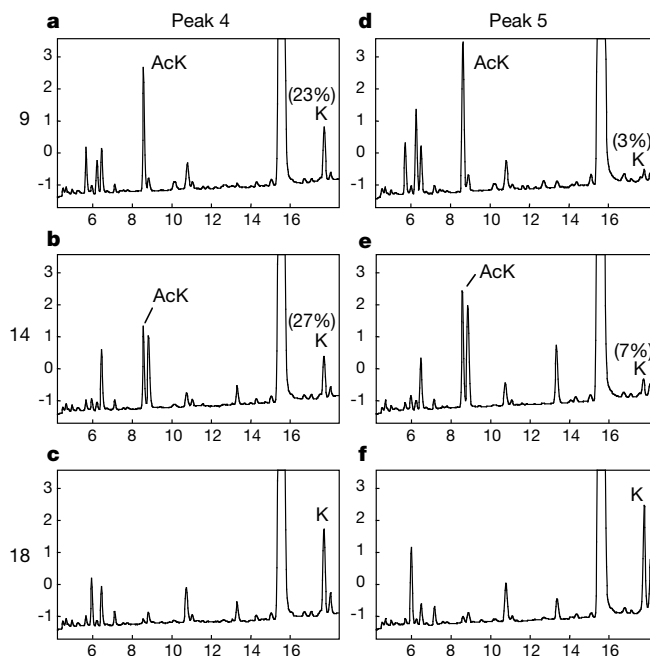


**Figure 2** Amino-terminal sequencing of peaks 4 and 5 of the Sir2 deacetylase reaction at 1 mM NAD as determined by Edman degradation. Chromatograms at positions 9 (**a,d**), 14 (**b,e**) and 18 (**c,f**) are shown. In peak 4, about 23% of Lys 9 (**a**) and 27% of Lys 14 (**b**) are deacetylated. In peak 5, Lys 9 and Lys 14 are essentially fully acetylated (**d,e**).

Unacetylated Lys 18 of peaks 4 and 5 is shown for comparison (**c,f**). The peak to the right of the acetylated lysine at position 14 corresponds to the chromatographic position of alanine, and represents a preview of Ala 15 in cycle 14.

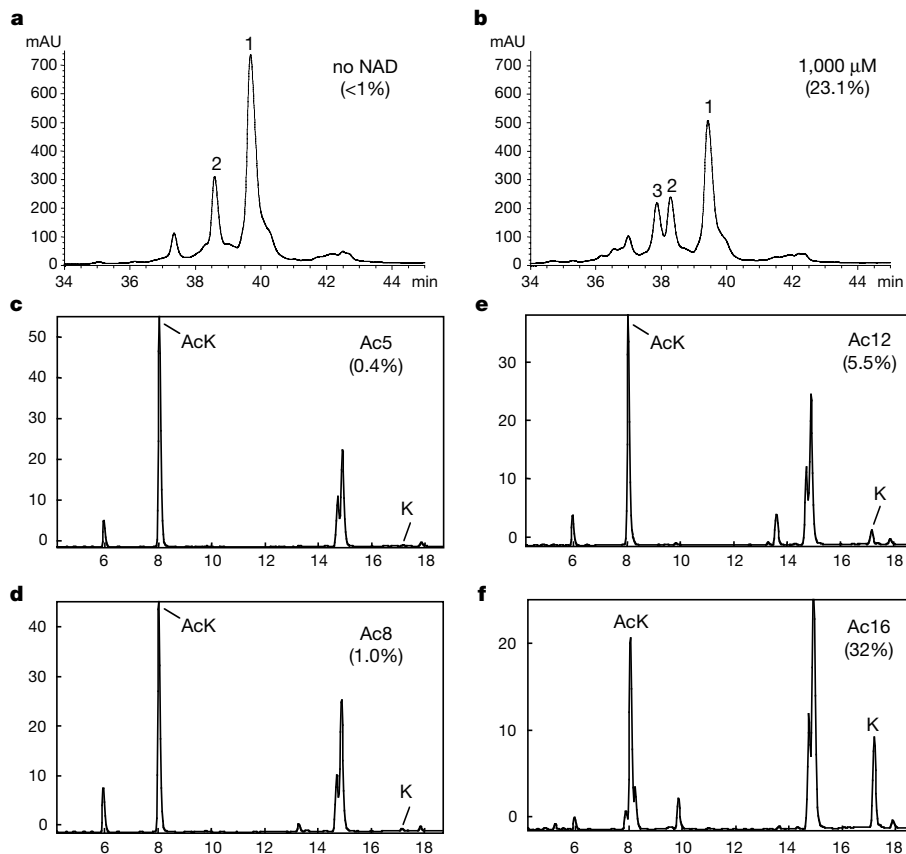


**Figure 3** The deacetylation activity of yeast Sir2 on the H4 peptide (residues 2–19) tetra-acetylated at lysines 5, 8, 12 and 16. **a,b**, HPLC chromatograms of products of deacetylation assays with Sir2 and the indicated concentrations of NAD. The efficiencies of the reactions are calculated from the areas under peaks. Peaks 1 and 2 correspond to the dimeric and monomeric forms, respectively, of the input peptide. Peak 3 corresponds to the deacetylated product. **c–f**, Amino-terminal sequencing of peak 3. Chromatograms

of positions 5, 8, 12 and 16 are shown. Substantial deacetylation (32%) is observed for only Lys16. The sum of deacetylation of all four residues, about 40%, is less than the theoretical 50% expected for the singly deacetylated dimeric peptide, most probably owing to contamination of peak 3 by peak 2. As a control, peak 1, corresponding to the original dimer peptide, shows minimal deacetylation at positions 5, 8, 12 and 16 (0.1%, 0.1%, 0.7% and 0.5%, respectively).

by Sir2. The concentration of NAD that allowed the reaction to proceed to ~50% of the maximal level was ~100  $\mu$ M.

To analyse these reaction products further, we subjected peak 4, the singly deacetylated dimer, along with the input peak 5, to N-terminal protein sequencing by Edman degradation (Fig. 2). The only differences between the input and reacted peaks occurred at lysines 9 and 14; 23–27% of the acetyl lysines at each position were deacetylated by Sir2 in the presence of NAD. Lysine 18 of peaks 4 and 5 was unacetylated. NADH, NADP and NADPH did not promote a significant level of deacetylation by Sir2, and neither NADH nor NADP inhibited the activity of NAD in this reaction (see Supplementary Information). Thus, Sir2 is an NAD-dependent histone deacetylase that can deacetylate either Lys 9 or Lys 14 of the H3 N-terminal tail. The number of moles of peptide deacetylated greatly exceeds that of Sir2, indicating that Sir2 catalyses multiple reaction cycles.

We then examined the Sir2 deacetylase activity using a 20-residue peptide of the N terminus of histone H4 completely acetylated at lysines 5, 8, 12 and 16 and containing a carboxyl cysteine. In the absence of NAD, this peptide gave rise to two prominent peaks (1 and 2) in HPLC corresponding to the dimeric and monomeric peptides, respectively (Fig. 3a). Addition of NAD elicited a third prominent peak (3, Fig. 3b) corresponding to a singly deacetylated species, which was collected and analysed by Edman degradation. Deacetylation selectively occurred at Lys 16 (Fig. 3c–f). About 32% of the Lys 16 was deacetylated as opposed to less than 6% of the other lysines. This specificity of Sir2 corresponds to the primary importance of Lys 16 of histone H4 in silencing.

We tested the effect of a potent inhibitor of histone deacetylases, trichostatin A (TSA)<sup>16</sup>. TSA was totally incapable of inhibiting deacetylation by Sir2 at 400 nM (Fig. 4a, b), a concentration that

inhibits histone deacetylases, including Rpd3 family members<sup>17</sup>. Consistent with its reported ADP-ribosyltransferase activity, Sir2 transferred <sup>32</sup>P from NAD to intact histone H3 (Fig. 4c) or to the di-acetylated H3 peptide (Fig. 4d). Transfer of label to the peptide was assayed using thin-layer chromatography (TLC), which revealed not only this transfer but also a substantial amount of NAD hydrolysis. We then tested a known inhibitor of mono-ADP-ribosyltransferases, coumermycin A1 (ref. 18). Both the ADP-ribosylation (Fig. 4c, d) and NAD hydrolysis (Fig. 4d) were inhibited by this drug at 200  $\mu$ M, a concentration that inhibits other mono-ADP-ribosyltransferases. Coumermycin A1 was not capable of inhibiting deacetylation of the H3 tail by Sir2 (Fig. 4e). Thus, the proposed activity of ADP-ribosyltransferase (and the NAD hydrolase) is fundamentally distinct from this NAD-dependent deacetylation activity.

We characterized a mouse Sir2 homologue called *mSir2 $\alpha$*  (GenBank accession number AF214646). The conserved region of this protein resembles yeast Sir2 more closely than do other mouse Sir2 proteins (Fig. 1h; and Supplementary Information). To determine whether the mouse Sir2 homologue *mSir2 $\alpha$*  would catalyse this deacetylation reaction, we incubated purified recombinant *mSir2 $\alpha$*  with the di-acetylated H3 peptide and analysed the reaction products by HPLC (Fig. 1a, i). The murine protein gave rise to the same array of products with a similar yield to that of the yeast enzyme, suggesting that mammalian Sir2 proteins are also mediators of transcriptional silencing.

To determine whether the histone deacetylase activity of Sir2 is required for *in vivo* functions, two alanine mutations in highly conserved residues of the core domain (Gly 270 and Asn 345) were introduced by site-directed mutagenesis (Fig. 5Aa). Six-histidine-tagged proteins were purified from *Escherichia coli* (Fig. 5Ab) and assayed for deacetylase activity with the di-acetylated H3 peptide (Fig. 5Ac–f). Mutant 345 was inactive, providing strong evidence that the deacetylase activity is an inherent property of Sir2, whereas mutant 270 showed a high level of activity—about 80% of that of wild type. These proteins were also analysed for ADP-ribosyltransferase activity using the intact histone H3 as substrate (Fig. 5Ag). Mutant 345 was inactive and mutant 270 now displayed only a very weak activity, about 7% of that of wild type.

To examine the functions of these mutants *in vivo*, we used a yeast indicator strain in which the endogenous *SIR2* had been deleted and the wild-type or mutant *SIR2* genes were integrated back into the genome. The mutant proteins were stably expressed (Fig. 5Ba). Silencing of the *HML $\alpha$*  locus was assayed by mating with a haploid strain of opposite mating type and monitoring the appearance of diploids on selective media (Fig. 5Bb). Mutant 270 was mating proficient, which indicates that silencing was intact, and mutant 345 was defective. Telomere silencing was determined by repression of the telomere-positioned *URA3* gene on media containing 5-fluoro-orotic acid (FOA), and this assay showed that mutant 270 had partial silencing and 345 was defective (Fig. 5Bc). Silencing in the rDNA was determined by repression of rDNA-positioned *ADE2* on adenine-free media, showing that mutant 270 silenced as well as the wild type, and that mutant 345 was defective (Fig. 5Bd).

Recombination in the rDNA was assayed by loss of *ADE2* on media limiting in adenine, giving rise to a red pigment. Half-red/white sector colonies indicate *ADE2* loss in the first generation after plating, and the frequency of these colonies compared with *Ade*<sup>+</sup> colonies is a direct measure of the recombination rate in the rDNA. Wild-type *SIR2* suppressed recombination about 12-fold compared with the *sir2* deletion strain; mutant 270 showed a high degree of suppression in the range of wild type; and mutant 345 was as defective as the *sir2* deletion (Fig. 5Be). Replicative life spans were also determined as another measure of *SIR2* function in the rDNA (Fig. 5Bf). The *sir2* deletion shortened life span about 50% as compared with wild type, as expected. Mutant 270 complemented the *sir2* deletion to give a wild-type life span and mutant 345 was completely defective in complementing the life span defect.

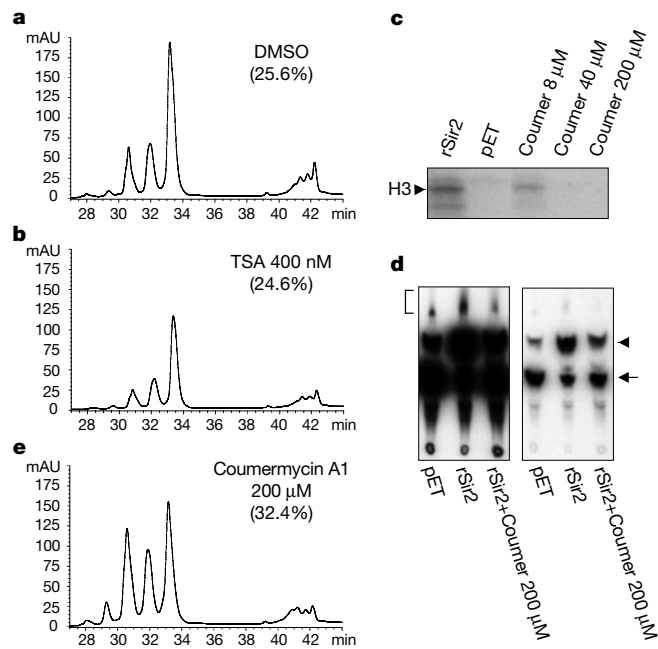


**Figure 4** Effects of inhibitors on the deacetylase and ADP-ribosyltransferase activities of recombinant Sir2 (rSir2). HPLC chromatograms of deacetylation reactions at 1 mM NAD in the presence of solvent only (a), 400 nM trichostatin A (TSA) (b), and 200  $\mu$ M coumermycin A1 (Coumer) (e) are shown. The calculated efficiencies of the reactions are indicated. The effect of 200  $\mu$ M coumermycin A1 on ADP-ribosylation at 1  $\mu$ M NAD of the intact histone H3 (c) and the H3 peptide (d) were examined on SDS–PAGE and TLC, respectively. pET corresponds to the vector control. In d, the ADP-ribosylated peptide is indicated by a bracket on a longer exposure (left), and NAD and its hydrolysed product are indicated by an arrow and an arrowhead, respectively, on a shorter exposure (right).

Although NAD and NADH are frequent enzyme co-factors in oxidation/reduction reactions, this is the first example in eukaryotes, to our knowledge, in which NAD drives a distinct enzymatic reaction, in other words, deacetylation by Sir2 of lysines in the N-terminal tails of histones H3 and H4. Our findings are consistent with studies that show the importance of lysines 9 and 14 in the tail of histone H3, and, most critically, of Lys 16 of H4, in silencing<sup>7-9</sup>. We suggest that deacetylation by Sir2 of Lys 16 of H4, and lysines 9 and 14 of H3 is essential for silencing, and deacetylation of other lysines in these histone tails may be a passive consequence of residence in silent chromatin.

What is the relationship between histone deacetylation and ADP-ribosylation? It has been reported that the ADP-ribosyltransferase activity of Sir2 is essential for silencing *in vivo*<sup>15</sup>. Backing this claim was the finding that Sir2 mutant H364Y loses ADP-ribosyltransferase activity *in vitro* and fails to support silencing *in vivo*. However, we find that mutation of this same histidine also greatly reduces the

NAD-dependent deacetylase activity (data not shown), much like our Asn 345 mutant. Moreover, the Gly 270 mutant, which is highly defective for ADP-ribosyltransferase but retains 80% of the wild-type deacetylase activity, is mostly proficient for silencing, recombination suppression and life span extension *in vivo*. Therefore, we surmise that the NAD-dependent deacetylase has a vital role in these Sir2 functions *in vivo*, whereas the ADP-ribosyltransferase does not. Sir2 proteins are known to move to sites of DNA breaks<sup>19,20</sup> to aid their repair by non-homologous end joining<sup>21,22</sup>. We propose that the ADP-ribosyltransferase activity of Sir2 may function in DNA repair. Consistent with this hypothesis are the observations that the ADP-ribosylation of histones occurs when cells are treated with DNA damaging agents<sup>23-25</sup> and antibodies against mono-ADP-ribose react with mammalian nuclei only when cells are treated with DNA-damaging agents<sup>26</sup>.

The NAD requirement of Sir2 for deacetylation suggests that this protein may be a sensor of the energy or oxidation state of cells. It is

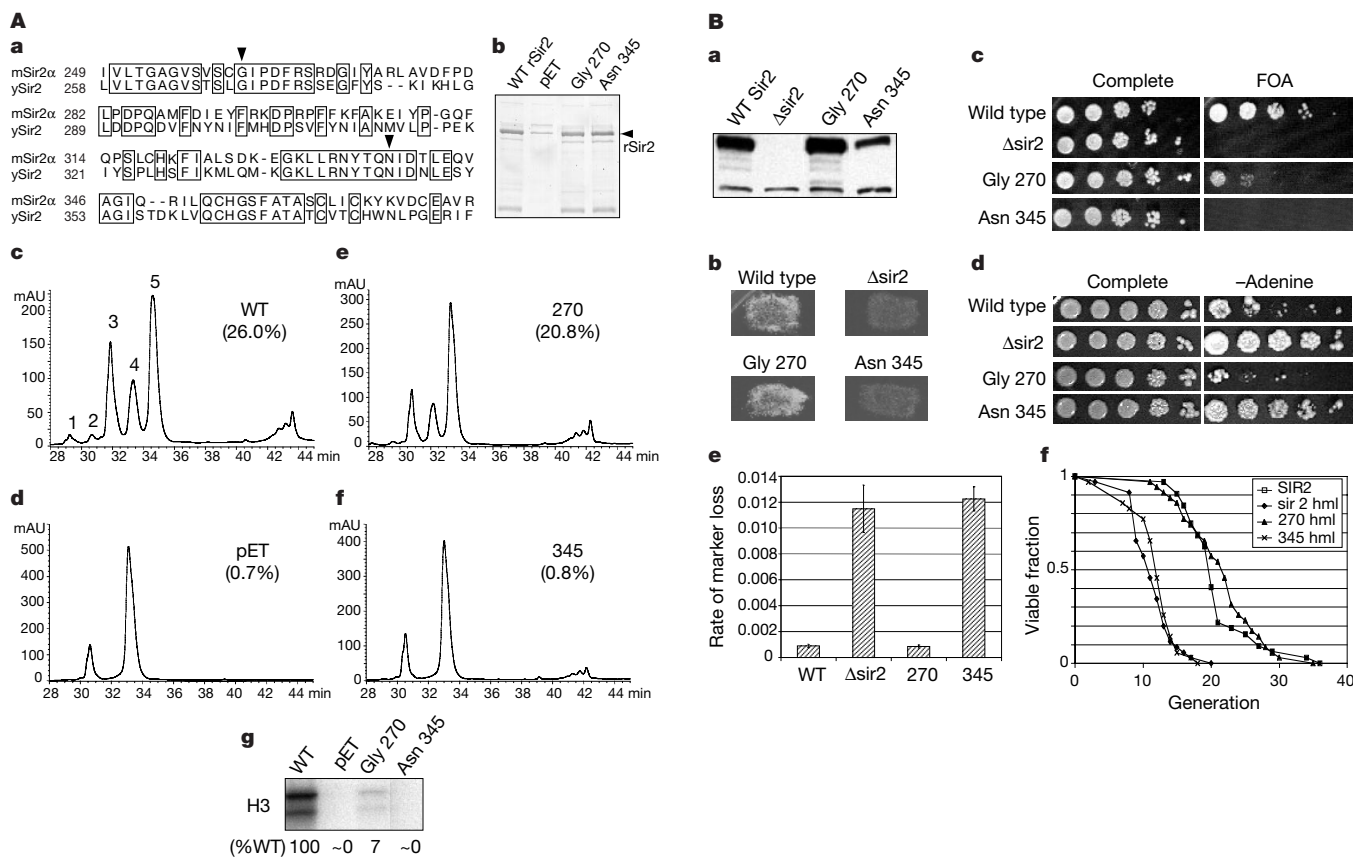


**Figure 5** Deacetylation activity of Sir2 is essential for silencing, recombination suppression and life-span extension *in vivo*. **A**, *In vitro* assays of Sir2 enzymatic activities. **a**, Two highly conserved residues (Gly 270 and Asn 345) between yeast Sir2 and mSir2 $\alpha$  (indicated by arrowheads) were mutated to alanine. **b**, 6  $\times$  His-tagged versions of wild-type and mutant Sir2 proteins along with a vector control (pET) were expressed in *E. coli*, purified over a Ni-NTA column and separated on a 7% polyacrylamide SDS gel stained with Coomassie blue. **c-f**, Effects of mutations in Sir2 on NAD-dependent histone H3 deacetylation activity. Indicated recombinant Sir2 proteins and a vector control were incubated with a peptide corresponding to the di-acetylated N-terminal tail of histone H3 and 1 mM NAD. HPLC chromatograms (absorbance at 220 nm) and efficiencies of the reactions are shown. **g**, Effects of mutations in Sir2 on ADP-ribosylation activity; 1  $\mu$ g of purified proteins were tested for the ability to ADP-ribosylate intact histone H3 with <sup>32</sup>P-labelled NAD. Lower band corresponds to a degraded histone product. Reaction efficiencies determined by phosphorimager quantitation are shown below. **B**, *In vivo* assays for SIR2 functions. **a**, Western blot of 25  $\mu$ g yeast whole-cell extracts from wild type, *sir2* $\Delta$  and the two mutants was performed using an anti-Sir2 antibody. The upper

band corresponds to Sir2 and a lower background band is included as a loading control. **b**, Silencing at *HML* $\alpha$  was tested by mating the strains with a tester strain of the opposite mating type and monitoring growth of diploids on selective media. **c**, Telomere silencing was assayed by the ability of strains with telomeric *URA3* to grow on media containing 5-FOA, which is toxic when *URA3* is expressed, but harmless when *URA3* is silenced. Strains were spotted in 10-fold dilutions on media lacking FOA (complete) and containing FOA. **d**, rDNA silencing was monitored in a strain with the *ADE2* marker located within the rDNA array. *RPD3* was disrupted to enhance silencing differences between wild-type and *sir2* $\Delta$  strains. *sir2* mutant strains were spotted in 10-fold dilutions on complete and adenine-minus media to monitor effects on silencing. **e**, W303R with *ADE2* at the rDNA was tested for rDNA recombination rates by counting the number of half-sectoring colonies lacking the marker in the first generation after plating. **f**, The mother cell life span of wild-type, *sir2* $\Delta$ , and mutants 270 and 345 were determined in *hml* $\Delta$  strains in which *a*/ $\alpha$  effects are eliminated. Co-expression of **a** and  $\alpha$  mating type genes has been shown to shorten life span in W303 (ref. 6).

interesting to note that the anti-ageing regimen of caloric restriction is effective in extending life span in a variety of organisms, including yeast<sup>27</sup>, *Caenorhabditis elegans*<sup>28</sup>, rodents<sup>29</sup> and probably primates<sup>30</sup>. We speculate that the slower metabolic rate in energy-deprived cells may exert part of its effect by increasing the availability of NAD, which, in turn, upregulates the deacetylation activity of Sir2 proteins and chromatin silencing. This persistence of genomic silencing may slow ageing-related processes, such as genomic instability and inappropriate gene expression. □

## Methods

### Production of recombinant proteins

The yeast *SIR2* gene or the *mSir2α* full-length cDNA was engineered to be cloned into pET28a vector (Novagen). Site-directed mutations were generated in the plasmid pRS305-SIR2 using the Gene Editor system (Promega) according to manufacturer's instructions. Sequences were verified by Sanger sequencing methods. The mutants were subcloned into pET28a. BL21(DE3) and BL21(DE3)pLysS with an extra copy of arginine transfer RNA gene were transformed with the *SIR2* and *mSir2α* plasmids, respectively. Each transformed bacterial clone was induced in 1 mM IPTG at 37 °C for 1 h. The induced 6 × His-tagged proteins were purified with Ni-NTA agarose under native conditions. The control eluate was prepared from a bacterial clone carrying pET28a vector only. The recombinant proteins were aliquoted and kept at -70 °C.

### Deacetylation and ADP-ribosylation assays

The typical reaction of Sir2 deacetylase activity was performed in 50 μl of buffer containing 50 mM Tris-HCl, pH 9.0, 4 mM MgCl<sub>2</sub>, 0.2 mM dithiothreitol (DTT), a variable concentration of unlabelled nicotinamide adenine dinucleotide (NAD) or NAD derivatives (Sigma, 5–10 μg of the purified recombinant Sir2 proteins and 10 μg of the N-terminal tail peptide of histone H3 (residues 1–20 + Cys; ARTKQTAR(AcK)STG-G(AcK)APRKQLC) di-acetylated at positions 9 and 14 or of *Tetrahymena* histone H4 (residues 2–19 + Cys; AGG(AcK)GG(AcK)GMG(AcK)VGA(AcK)RHSC) tetra-acetylated at positions 5, 8, 12 and 16 (Upstate Biotechnology). The starting peptide material of H3 contains a contaminant with a relative molecular mass 100 smaller, which also showed exactly the same patterns of deacetylation (data not shown). To detect the ADP-ribosylation activity, 8 μCi of NAD 5'-[α-<sup>32</sup>P]triphosphate (~1,000 Ci mmol<sup>-1</sup>, Amersham Pharmacia) was added to the same reaction containing 1 μM unlabelled NAD. Four micrograms of intact histone H3 protein (Roche Molecular Biochemicals) was also used for this assay. All reaction mixtures were incubated at room temperature for 1 h. Trichostatin A and coumermycin A1 (Sigma) were prepared in dimethylsulphoxide (DMSO), and 5 μl of solvent or inhibitor was added to the reactions before adding Sir2 proteins.

### Analysis of deacetylated or ADP-ribosylated products

After the incubation, the products were precipitated at -20 °C overnight by adding 50 μl of distilled water and 25 μl of 100% trichloroacetic acid (TCA) solution. For HPLC, the precipitates were reconstituted in 5% CH<sub>3</sub>CN and 0.1% trifluoroacetic acid (TFA) and run through a gradient concentration of 0.05% TFA to 0.043% TFA plus 80% CH<sub>3</sub>CN on Hewlett Packard Model 1100 HPLC system with 214TP52 column (Vydac). The chromatograms (absorbance measured at 210 nm) were digitally recorded and analysed by Hewlett Packard ChemStation system (version A.06.03(509)). Fractions of samples were collected every 1 min by Gilson Fraction Collector Model 203. Peptide sequencing was done by the Applied Biosystems Precise 494 HT protein sequencing system. PTH amino-acid chromatograms were recorded and analysed by the ABI Model 610A2.1 data integration/analysis system. Electron-spray mass spectroscopy was done on the PE Sciex Model API365 system. The mass spectroscopy data were analysed by the BioMultiView program (version 1.3.1). To detect the ADP-ribosylated intact H3 protein, the pellets were dissolved in 15 μl of Laemmli's sample buffer, boiled for 1.5 min and electrophoresed in a 10–20% gradient SDS-PAGE gel. The gel was stained with Coomassie Brilliant Blue to check equal loading of histones, dried and exposed to Kodak X-OMAT film. To analyse the ADP-ribosylated H3 peptides, 10 μl of each reaction mixture was spotted on a cellulose TLC plate (EM Science). Chromatography was carried out for 9–10 h in a TLC chamber containing a 65:5:3:2:29 mixture of isobutyric acid, pyridine, acetic acid, butanol and water. The plate was dried and exposed to Kodak X-OMAT film. Peptide spots were checked by ninhydrin staining.

### Molecular cloning of mSir2α

The mouse 15-day embryo 5'-STRETCH PLUS cDNA library (Clontech) was screened with the expressed sequence tag cDNA fragment of AA199012 as a probe. Five positive clones were obtained from roughly one-million independent plaques. One of the five clones contained a 3.9-kb cDNA fragment. The nucleotide sequence of this fragment was determined with an Applied Biosystems 374 automated sequencer. We concluded that the cDNA clone that we isolated encodes the full-length mSir2α protein, because the *in vitro* translated protein from this cDNA clone had an *M<sub>r</sub>* (110–120K) indistinguishable from that of the protein in the mouse NIH3T3 extract recognized by a specific polyclonal antibody against a N-terminal portion of mSir2α (data not shown). The amino-acid sequences of mSir2α and other *SIR2* family members were aligned in the Clustal X program and a phylogenetic tree was generated by using the NJPLOT program (see Supplementary Information).

### Strains, plasmids and antibodies

All strains used were derivatives of W303a *sir2Δ*: W303R *sir2Δ*(*MATa*, *ade2-1*, *leu2-3,112*, *trp1-1*, *ura3-52*, *his3-11*, *sir2::TRP1*, *rDNA-ADE2*), W303RT *sir2Δ*(*MATa*, *ade2-1*, *leu2-3,112*, *trp1-1*, *ura3-52*, *his3-11*, *rad5-535*, *sir2::TRP1*, *rDNA-ADE2*, *TELVIII-URA3*), and W303R *sir2Δ/rpd3Δ*(*MATa*, *ade2-1*, *leu2-3,112*, *trp1-1*, *ura3-52*, *his3-11*, *rpd3::URA3*, *sir2::TRP1*, *rDNA-ADE2*). We used pRS305-SIR2, an integrating plasmid that contains *SIR2* driven by its native promoter. Mutant *SIR2* genes were also cloned into these vectors. *SIR2* and mutant *sir2* strains were generated by cutting the plasmid within the *LEU2* gene and integrated using standard yeast transformation protocols. Rabbit antibodies against Sir2 were generated by using full-length recombinant Sir2 purified under denaturing conditions.

### Silencing, life span and rDNA recombination assays

To test silencing at the telomeres and rDNA, 10-fold dilutions of the derivatives of W303RT and W303R *Δrpd3* were spotted on media containing 5-FOA and media lacking adenine, respectively. To assay for HM silencing, W303R derivatives were spotted onto YPD with the tester strain CKy20 (*MATα*, *arg1*, *ism11*) and after overnight growth were replica plated to minimal media with no supplemented amino acids. Life span and rDNA recombination rates were measured as described<sup>6</sup>.

Received 2 December 1999; accepted 26 January 2000.

- Rine, J. & Herskowitz, I. Four genes responsible for a position effect on expression from *HML* and *HMR* in *Saccharomyces cerevisiae*. *Genetics* **116**, 9–22 (1987).
- Gottschling, D. E., Aparicio, O. M., Billington, B. L. & Zakian, V. A. Position effect at *S. cerevisiae* telomeres: reversible repression of Pol II transcription. *Cell* **63**, 751–762 (1990).
- Bryk, M. *et al.* Transcriptional silencing of Ty1 elements in the RDN1 locus of yeast. *Genes Dev.* **11**, 255–269 (1997).
- Smith, J. S. & Boeke, J. D. An unusual form of transcriptional silencing in yeast ribosomal DNA. *Genes Dev.* **11**, 241–254 (1997).
- Gottlieb, S. & Esposito, R. E. A new role for a yeast transcriptional silencer gene, *SIR2*, in regulation of recombination in ribosomal DNA. *Cell* **56**, 771–776 (1989).
- Kaerberlein, M., McVey, M. & Guarente, L. The *SIR2/3/4* complex and *SIR2* alone promote longevity in *Saccharomyces cerevisiae* by two different mechanisms. *Genes Dev.* **13**, 2570–2580 (1999).
- Thompson, J. S., Ling, X. & Grunstein, M. Histone H3 amino terminus is required for telomeric and silent mating locus repression in yeast. *Nature* **369**, 245–247 (1994).
- Hecht, A., Laroche, T., Strahl-Bolsinger, S., Gasser, S. M. & Grunstein, M. Histone H3 and H4 N-termini interact with SIR3 and SIR4 proteins: A molecular model for the formation of heterochromatin in yeast. *Cell* **80**, 583–592 (1995).
- Braunstein, M., Sobel, R. E., Allis, C. D., Turner, B. M. & Broach, J. R. Efficient transcriptional silencing in *Saccharomyces cerevisiae* requires a heterochromatin histone acetylation pattern. *Mol. Cell Biol.* **16**, 4349–4356 (1996).
- Braunstein, M., Rose, A. B., Holmes, S. G., Allis, C. D. & Broach, J. R. Transcriptional silencing in yeast is associated with reduced nucleosome acetylation. *Genes Dev.* **7**, 592–604 (1993).
- Sinclair, D. A. & Guarente, L. Extrachromosomal rDNA circles—a cause of aging in yeast. *Cell* **91**, 1–20 (1997).
- Brachmann, C. B. *et al.* The *SIR2* gene family, conserved from bacteria to humans, functions in silencing, cell cycle progression, and chromosome stability. *Genes Dev.* **9**, 2888–2902 (1995).
- Tsang, A. W. & Escalante-Semerena, J. C. CobB, a new member of the SIR2 family of eucaryotic regulatory proteins, is required to compensate for the lack of nicotinate mononucleotide:5,6-dimethylbenzimidazole phosphoribosyltransferase activity in *cobT* mutants during cobalamin biosynthesis in *Salmonella typhimurium* LT2. *J. Biol. Chem.* **273**, 31788–31794 (1998).
- Frye, R. A. Characterization of five human cDNAs with homology to yeast SIR2 gene: Sir2-like proteins (Sirtuins) metabolize NAD and may have protein ADP-ribosyltransferase activity. *Biochem. Biophys. Res. Commun.* **260**, 273–279 (1999).
- Tanny, J. C., Dowd, G. J., Huang, J., Hiltz, H. & Moazed, D. An enzymatic activity in the yeast Sir2 protein that is essential for gene silencing. *Cell* **99**, 735–745 (1999).
- Yoshida, M., Kijima, M. & Akita, M. & Beppu, T. Potent and specific inhibition of mammalian histone deacetylase both *in vivo* and *in vitro* by Trichostatin A. *J. Biol. Chem.* **265**, 17174–17179 (1990).
- Taunton, J., Hassig, C. A. & Schreiber, S. L. A mammalian histone deacetylase related to the yeast transcriptional regulator Rpd3p. *Science* **272**, 408–411 (1996).
- Banasik, M. & Ueda, K. Inhibitors and activators of ADP-ribosylation reactions. *Mol. Cell Biochem.* **138**, 185–197 (1994).
- Mills, K. D., Sinclair, D. A. & Guarente, L. *MEC1*-dependent redistribution of the Sir3 silencing protein from telomeres to DNA double-strand breaks. *Cell* **97**, 609–620 (1999).
- Martin, S. G., Laroche, T., Suka, N., Grunstein, M. & Gasser, S. M. Relocalization of telomeric Ku and SIR proteins in response to DNA strand breaks in yeast. *Cell* **97**, 621–633 (1999).
- Boulton, S. J. & Jackson, S. P. Identification of a *Saccharomyces cerevisiae* Ku80 homolog: roles in DNA double strand break rejoining and in telomeric maintenance. *Nucleic Acids Res.* **24**, 4639–4648 (1998).
- Tsukamoto, Y., Kato, J. & Ikeda, H. Silencing factors participate in DNA repair and recombination in *Saccharomyces cerevisiae*. *Nature* **388**, 900–903 (1997).
- Adamietz, P. & Rudolph, A. ADP-ribosylation of nuclear proteins *in vivo*: identification of histone H2B as a major acceptor for mono- and poly(ADP-ribose) in dimethyl sulfate-treated hepatoma AH7974 cells. *J. Biol. Chem.* **259**, 6841–6846 (1984).
- Kreimeyer, A., Wielckens, K., Adamietz, P. & Hiltz, H. DNA repair-associated ADP-ribosylation *in vivo*: modification of histone H1 differs from that of the principal acceptor proteins. *J. Biol. Chem.* **259**, 890–896 (1984).
- Pero, R. W., Holmgren, K. & Persson, L. Gamma-radiation induced ADP-ribosyltransferase activity and mammalian longevity. *Mutat. Res.* **142**, 69–73 (1985).
- Meyer, T. & Hiltz, H. Production of anti-(ADP-ribose) antibodies with the aid of a dinucleotide-pyrophosphatase-resident hapten and their application for the detection of mono(ADP-ribose)lated polypeptides. *Eur. J. Biochem.* **155**, 157–165 (1986).

27. Muller, I., Zimmermann, M., Becker, D. & Flomer, M. Calendar life span versus budding life span of *Saccharomyces cerevisiae*. *Mech. Ageing Dev.* **12**, 47–52 (1980).
28. Lakowski, B. & Hekimi, S. The genetics of caloric restriction in *Caenorhabditis elegans*. *Proc. Natl Acad. Sci. USA* **95**, 13091–13096 (1998).
29. Weindruch, R. H., Walford, R. L., Fligiel, S. & Guthrie, D. The retardation of aging in mice by dietary restriction: Longevity, cancer, immunity, and lifetime energy intake. *J. Nutr.* **116**, 641–654 (1986).
30. Roth, G. S. Calorie restriction in primates: will it work and how will we know? *J. Am. Geriatr. Soc.* **47**, 896–903 (1999).

Supplementary information is available on Nature's World-Wide Web site (<http://www.nature.com>) or as paper copy from the London editorial office of Nature.

Acknowledgements

We thank R. Cook, A. Park, and H. Amoroso at the MIT Biopolymers lab for the HPLC and electron-spray mass spectroscopy, and P. Matsudaira for the MALDI mass spectroscopy. We also thank S. Inamoto for bacterial strains, and H. Tissenbaum and E. Ford for comments on the paper. This work was funded by The Human Frontier Science Program Organization Long-Term Fellowship to S. I., a NIH predoctoral grant to C.A. and M.K., and grants from the NIH, Seaver Foundation, Ellison Medical Foundation, and Howard and Linda Stern Fund to L.G.

Correspondence and requests for materials should be addressed to L.G. (e-mail: leng@mit.edu.)

The structures of HslU and the ATP-dependent protease HslU–HslV

Matthias Bochtler\*†, Claudia Hartmann\*†, Hyun Kyu Song\*, Gleb P. Bourenkov‡, Hans D. Bartunik‡ & Robert Huber\*

\* Max-Planck-Institut für Biochemie, Am Klopferspitz 18a, D-82152 Martinsried, Planegg, Germany

‡ Arbeitsgruppen für strukturelle Molekularbiologie der Max-Planck-Gesellschaft, Notkestr. 85, D-22603 Hamburg, Germany

† These authors contributed equally to this work

The degradation of cytoplasmic proteins is an ATP-dependent process<sup>1</sup>. Substrates are targeted to a single soluble protease, the 26S proteasome<sup>2,3</sup>, in eukaryotes and to a number of unrelated proteases in prokaryotes<sup>4,5</sup>. A surprising link emerged with the discovery of the ATP-dependent protease HslVU (heat shock locus VU)<sup>6–8</sup> in *Escherichia coli*. Its protease component HslV shares ~20% sequence similarity<sup>6</sup> and a conserved fold<sup>9</sup> with 20S proteasome  $\beta$ -subunits. HslU is a member of the Hsp100 (Clp) family of ATPases. Here we report the crystal structures of free HslU and an 820,000 relative molecular mass complex of HslU and HslV—the first structure of a complete set of components of an ATP-dependent protease. HslV and HslU display sixfold symmetry, ruling out mechanisms of protease activation that require a symmetry mismatch between the two components. Instead, there is conformational flexibility and domain motion in HslU and a localized order–disorder transition in HslV. Individual subunits

of HslU contain two globular domains in relative orientations that correlate with nucleotide bound and unbound states. They are surprisingly similar to their counterparts in N-ethylmaleimide-sensitive fusion protein<sup>10,11</sup>, the prototype of an AAA-ATPase. A third, mostly  $\alpha$ -helical domain in HslV mediates the contact with HslU and may be the structural equivalent of the amino-terminal domains in proteasomal AAA-ATPases.

We expressed and purified histidine-tagged variants of HslV and HslU from *E. coli*. Mixing the two components was sufficient to recover ATP-dependent protease activity, as assessed by enzymatic assay with both the chromogenic peptide Z-GGL-AMC<sup>7</sup> and radio-labelled <sup>14</sup>C-methylcasein<sup>12</sup>; the latter was used as a model system for large, denatured proteins (data not shown). Three crystal forms grew (Fig. 1; and Table 1). The crystals of space group P6<sub>3</sub>22 contain free HslV and HslV–HslU fully bound with AMP-PNP (5'-adenylylimidotriphosphate) on 32-point symmetry positions (Fig. 1a). In the absence of both HslV and exogenous nucleotide, HslU crystallized in space group P2<sub>1</sub>2<sub>1</sub>2, with a full hexamer in the asymmetric unit. Four subunits are complexed with nucleotide, presumably from the cellular environment. The remaining two subunits are located on opposite sides of the ring and contain bound sulphate from the crystallization buffer (Fig. 1b). The addition of the non-hydrolysable AMP-PNP induced the growth of trigonal crystals under identical conditions with two independent hexamers located on threefold crystallographic axes with nucleotide bound to alternating subunits on the ring (Fig. 1c). Empty subunits have been modelled without sulphate and show local main-chain conformational changes of the phosphate-binding loop (P-loop).

High sequence similarity predicts that there is a conserved fold in all members of the Hsp100 (Clp) family of ATPases. In contrast, the identification of the Hsp100s as AAA proteins<sup>13</sup> has been controversial<sup>14</sup>. Comparison of the HslU structure with the only atomic-resolution structure of an AAA protein available so far<sup>10,11</sup> strongly supports this classification (see Fig. 2). HslU is folded into three distinct domains. We observe the same topology in the N-terminal domain (D2) of N-ethylmaleimide-sensitive fusion (NSF) protein and the N-terminal domain of HslU. In HslU, this domain comprises residues S2–K109 and I244–L332 and will be referred to as the N domain. Residues M110 to A243 are missing in other Hsp100 proteins and emerge from the globular domain. The structural equivalence of the HslU and NSF D2 backbones is greatest (r.m.s. deviation of C $\alpha$  bond lengths = 0.7Å) for a central, parallel  $\beta$ -sheet that forms the core of the protein in both structures, having strand order  $\beta$ N2,  $\beta$ N3,  $\beta$ N6,  $\beta$ N1,  $\beta$ N7 in HslU (see Fig. 2; and Table 2). C $\alpha$  carbons of corresponding residues in the sequence alignment are nearly coincident, with the exception of residues PFIK of strand  $\beta$ N2 in HslU, which correspond to residues FIKI in NSF. Lysine 80 is extended towards the nucleotide in HslU. The central  $\beta$ -sheet in both HslU and NSF is sandwiched in between two layers of  $\alpha$ -helices as in other P-loop proteins. The P-loop is located between strand  $\beta$ N1 and helix  $\alpha$ N4 in HslU and is in contact with nucleotide as expected<sup>15,16</sup>. As in NSF, and unlike in other P-loop triphosphate

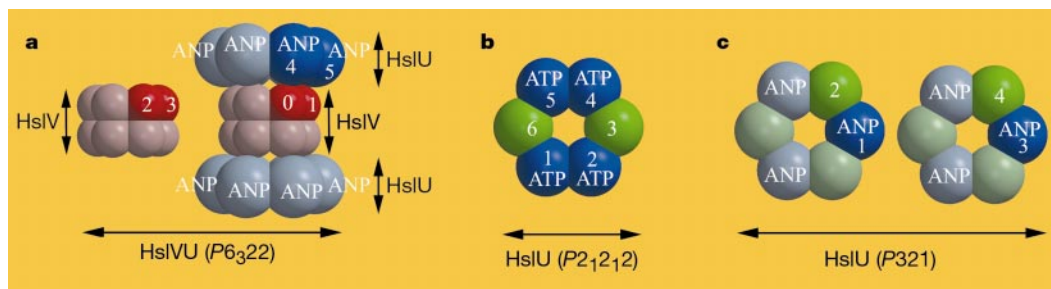


Figure 1 Summary of the three crystal forms (a–c) that were used for structure determination. Subunits in the respective asymmetric units are numbered 1–6.